

## Article

# Heterostructural Mixed Oxides Prepared via ZnAlLa LDH or ex-ZnAl LDH Precursors—Effect of La Content and Its Incorporation Route

Katarzyna Antoniak-Jurak <sup>1,\*</sup> , Paweł Kowalik <sup>1</sup>, Wiesław Próchniak <sup>1</sup>, Robert Bicki <sup>1</sup>  and Grzegorz Słowik <sup>2</sup> 

<sup>1</sup> Catalysts Department, Łukasiewicz Research Network-New Chemical Syntheses Institute, Al. Tysiąclecia Państwa Polskiego 13A, 24-110 Puławy, Poland; pawel.kowalik@ins.lukasiewicz.gov.pl (P.K.); wieslaw.prochniak@ins.lukasiewicz.gov.pl (W.P.); robert.bicki@ins.lukasiewicz.gov.pl (R.B.)

<sup>2</sup> Department of Chemical Technology, Institute of Chemical Sciences, Faculty of Chemistry, Maria Curie-Skłodowska University in Lublin, Maria Curie-Skłodowska Sq. 3, 20-031 Lublin, Poland; grzegorz.slowik@poczta.umcs.lublin.pl

\* Correspondence: katarzyna.antoniak@ins.lukasiewicz.gov.pl; Tel.: +48-8-1473-1754

**Abstract:** The effect of La content and its incorporation route on physicochemical properties of ZnO/Zn(Al,La)<sub>2</sub>O<sub>4</sub> or La<sub>2</sub>O<sub>3</sub>-ZnO/ZnAl<sub>2</sub>O<sub>4</sub> mixed oxides with a spinel structure obtained from ZnAlLa Layered double hydroxides (LDHs) or ex-ZnAl LDH materials was investigated. The heterostructural nanocomposites with the similar Zn/Al molar ratio and varied La content were prepared by two techniques: via co-precipitation and thermal treatment of ZnAlLa LDHs at 500 °C or via incipient wetness impregnation of ex-ZnAl LDHs with aqueous solutions of lanthanum nitrate and subsequent thermal treatment. The obtained series of materials were characterized by the following techniques: X-ray fluorescence (XRF), N<sub>2</sub> adsorption (BET), X-ray diffraction (XRD), Fourier-transform infrared spectroscopy (FT-IR), thermogravimetric analysis with evolved gas analysis (TG/DTG/EGA), scanning transmission electron microscopy (STEM) energy-dispersive X-ray spectroscopy (EDS), high-resolution transmission electron microscopy (HRTEM) and Fourier-transform infrared spectroscopy (FFT). The evaluation of activity toward the high-temperature water gas shift (HT-WGS) within the temperature range of 350–420 °C was carried out on the basis of rate constant measurements in the kinetic mode using a differential reactor. The co-precipitation technique allowed for a better distribution of La in bulk and on the spinel surface than in case of lanthanum incorporation via impregnation. ZnO/Zn(Al,La)<sub>2</sub>O<sub>4</sub> or La<sub>2</sub>O<sub>3</sub>-ZnO/ZnAl<sub>2</sub>O<sub>4</sub> mixed oxides were characterized by moderate activity in the HT-WGS reaction. The results reveal that introduction of lanthanum oxide over 2.4–2.8 wt% induces the phase separation of the ZnAl<sub>2</sub>O<sub>4</sub> spinel, forming ZnO on the ZnAl<sub>2</sub>O<sub>4</sub> spinel surface.

**Keywords:** non-stoichiometric zinc aluminate spinels; mixed metal oxides; heterostructural nanocomposites; surface reconstruction of ZnAl<sub>2</sub>O<sub>4</sub>



**Citation:** Antoniak-Jurak, K.; Kowalik, P.; Próchniak, W.; Bicki, R.; Słowik, G. Heterostructural Mixed Oxides Prepared via ZnAlLa LDH or ex-ZnAl LDH Precursors—Effect of La Content and Its Incorporation Route. *Materials* **2021**, *14*, 2082. <https://doi.org/10.3390/ma14082082>

Academic Editor: Mateusz Dulski

Received: 18 March 2021

Accepted: 17 April 2021

Published: 20 April 2021

**Publisher's Note:** MDPI stays neutral with regard to jurisdictional claims in published maps and institutional affiliations.



**Copyright:** © 2021 by the authors. Licensee MDPI, Basel, Switzerland. This article is an open access article distributed under the terms and conditions of the Creative Commons Attribution (CC BY) license (<https://creativecommons.org/licenses/by/4.0/>).

## 1. Introduction

Layered double hydroxides (LDHs) are commonly applied as catalyst supports, catalyst precursors and nanocatalysts [1–3]. The uniqueness of LDHs is associated with an easy anionic metal complexes incorporation into the interlayer galleries of regular arrangement. An additional advantage of LDHs is the ability to incorporate a wide range of various cations with a similar ionic radius, e.g., Mg<sup>2+</sup>, Cu<sup>2+</sup>, Ni<sup>2+</sup>, into the brucite-like layers [4]. During thermal treatment, they decompose forming nano-sized simple and mixed oxides with unique properties. The characteristic features of resulting materials are high specific surface area, homogeneous distribution of components (even on the atomic level) and the so called memory effect involving the recovery of the primary structure in contact with an aqueous salt solution [5].

Mixed Zn–Al oxides obtained from LDHs are used in a number of applications as sensors, high temperature ceramic material, photocatalysts [6], supports and catalysts for various chemical reactions [2]. In the preparation process, numerous synthesis methods are applied, i.e., coprecipitation [7,8], hydrothermal [9], microemulsion techniques [10], allowing to obtain the specific defective structures with enhanced catalytic properties [11]. Stability of ex-LDH catalytic systems can be increased by modification with rare earth metals (La, Ce) of low electronegativity [12]. Their presence reduces mobility of surface atoms and thus it stabilizes the catalyst structure. Lanthanum oxide is one of the most effective stabilizers of structural properties of metallic and oxide catalysts containing alumina, as it inhibits the phase transition of  $\gamma$ -Al<sub>2</sub>O<sub>3</sub> to  $\alpha$ -Al<sub>2</sub>O<sub>3</sub> [13]. According to Liu [14], it can be concluded that La is easily incorporated into the spinel-like structure of Mg<sub>x</sub>Al<sub>y</sub>O<sub>z</sub>. The consequence of this is the increase of an average pore size and durability in a steam-rich atmosphere. Similar effects of La doping may be expected in the case of spinel Zn<sub>x</sub>Al<sub>y</sub>O<sub>z</sub>.

In the preparation of ZnAlLa materials, numerous synthesis methods are applied. Xie et al. [15] studied systems with the same molar ratio ( $M^{2+}/M^{3+} = 2$ ) and variable La content ( $La^{3+}/Al^{3+}$  molar ratio in the range from 0 to  $\infty$ ) obtained using precipitation with sodium hydroxide (at low CO<sub>3</sub><sup>2-</sup> concentration in the reaction environment) at variable pH (ranging from 2 to 13) and then subjected to hydrothermal processing (110–140 °C) and calcination (100–700 °C). The other variant of Zn–Al–La synthesis was proposed by Liu [14]. That catalyst preparation route (molar ratio of Zn/Al = 0.5 and La content in the range of 1.5–30 wt%) involved coprecipitation of the hydroxycarbonate precursor at pH ranging from 8.0 to 9.0, removal of Na<sup>+</sup> and subsequent precursor calcination at 700 °C.

The catalytic effect of lanthanum-doped Zn–Al systems was also studied in esterification. According to Tzompantzi et al. [16,17] La incorporation at the stage of synthesis of Zn–Al–La LDHs via the urea route increases activity of the Zn–Al oxide catalyst towards the esterification reaction. The object of the study was systems with a constant Zn/Al = 2 molar ratio, in which the La share was up to 3 wt%. Oxide materials obtained by ZnAlLa LDH calcination at 400 °C displayed a significantly smaller surface area but increased pore volume with an increase in the La<sub>2</sub>O<sub>3</sub> content. A feature that particularly influences the better catalytic properties of Zn–Al–La systems in relation to the unmodified material is higher surface alkalinity, especially the presence of strongly alkaline surface centers. The authors of the paper explained the creation of such centers with the intensive interaction that occurred on the ZnO–La<sub>2</sub>O<sub>3</sub> interface. Their presence determines better catalytic properties of Zn–Al–La systems in the esterification reaction of oleic acid fatty grass and phenol photomineralization in comparison with Zn–Al systems.

Another approach to synthesis of the ZnAlLa nanospinel was presented by Shariatinia et al. [18] proposing the use of gel combustion with poly(vinyl alcohol) or glycerin to obtain Zn–Al–La expressed in the following molar ratios: Zn/Al = 2.2, La/Al = 2.5.

Attempts to obtain effective catalysts for methanol steam reforming based on Zn–Al–La systems and with the same composition and obtained analogously using gel combustion and then supported on cordierite structural reactors were carried out by Khani et al. [19,20]. Such systems display favorable thermal stability which is proved with a relatively low decrease of the specific surface area at high temperatures (1000 °C). Based on the Zn–Al–La spinel, the copper catalyst was prepared which, after placing it on a monolith, appeared to be highly effective in methanol steam reforming.

To the best of our knowledge, the catalytic properties of Zn–Al–La materials, especially the effect of lanthanum on the efficiency and durability at high-temperature water–gas shift (HT-WGS) conditions, have not been studied so far.

The water–gas shift reaction is an exothermic reaction, and CO conversion is favored at lower temperatures. The process is carried out to enrich the synthesis gas in hydrogen with the simultaneous removal of carbon dioxide according to the following reaction:  $CO + H_2O \rightleftharpoons CO_2 + H_2$  ( $\Delta H$  (298K) =  $-41.1$  kJ/mol). Usually, the WGS reaction is conducted in two adiabatic reactors arranged in series, which are the high-temperature WGS (HT-

WGS, 320–450 °C) and the low-temperature WGS (LT-WGS, 200–250 °C), to maximize the CO conversion. In our previous publication [21], it was shown that ecofriendly K-decorated mixed oxides (Zn–Al) with a spinel-type structure obtained via co-precipitation and thermal treatment of ZnAl LDHs (with compositions of  $(\text{Zn}/\text{Al})_{\text{mol}} = 0.3, 0.5$  and  $1.0$ ) catalyze the HT-WGS reaction effectively. The highest activity was found for the Zn/Al molar ratio of 0.5 corresponding to spinel stoichiometry. In spite of their high activity, potassium-promoted Zn–Al systems display different thermal stability. It seems that this fact can be related to alkali mobility and tendency to surface migration. The use of the heterostructural nanocomposite of ZnO/Zn(Al,La)<sub>2</sub>O<sub>4</sub> or La<sub>2</sub>O<sub>3</sub>–ZnO/ZnAl<sub>2</sub>O<sub>4</sub> allows for better stabilization of the alkali that are used as promoters of HT-WGS catalysts.

The presented work describes the effect of La content and its incorporation route on the physicochemical properties of ZnO/Zn(Al,La)<sub>2</sub>O<sub>4</sub> or La<sub>2</sub>O<sub>3</sub>–ZnO/ZnAl<sub>2</sub>O<sub>4</sub> mixed oxides with the spinel structure. Ternary Zn–Al–La oxide systems were prepared by coprecipitation and thermal treatment of ZnAlLa LDHs at 500 °C and via impregnation of ex-ZnAl LDHs with the lanthanum nitrate aqueous solution and subsequent thermal treatment at 500 °C. The obtained precursors and their calcination products were analyzed in terms of their physicochemical properties using X-ray fluorescence (XRF), N<sub>2</sub> adsorption (BET), X-ray diffraction (XRD), thermogravimetric analysis with evolved gas analysis (TG/DTG/EGA), scanning transmission electron microscopy (STEM)–energy-dispersive X-ray spectroscopy (EDS), Fourier-transform infrared spectroscopy (FT-IR), high-resolution transmission electron microscopy (HRTEM) and fast Fourier transform (FFT). The activity of ZnAl\_W<sub>k</sub>\_xLa and ZnAl\_I<sub>k</sub>\_xLa series was evaluated in the HT-WGS reaction.

## 2. Materials and Methods

### 2.1. Preparation of La-Doped Zn–Al Materials

Two series of La-modified Zn–Al materials were prepared.

Series I was prepared via co-precipitation and thermal treatment of ZnAlLa LDHs at 500 °C. Zn–Al–La LDH materials with a similar molar ratio of Zn/Al (~0.7) and with different nominal content of La (from 1 to 9 wt%) were prepared by coprecipitation method from aqueous solutions of zinc, aluminum and lanthanum nitrate with the aqueous solution of Na<sub>2</sub>CO<sub>3</sub> + NaOH at 75–80 °C and pH in the range of 7.5–8. After complete precipitation, the slurry was aged at 80 °C for 0.5 h under vigorous stirring. The solids obtained were thoroughly filtered and washed and then dried at 100 °C and subsequently calcined at 500 °C for 4 h. After drying, the prepared samples were marked with the following symbols: ZnAl\_W\_1La, ZnAl\_W\_2La, ZnAl\_W\_3La, ZnAl\_W\_4La, ZnAl\_W\_5La, and the corresponding calcination products were marked with the following symbols: ZnAl\_W<sub>k</sub>\_1La, ZnAl\_W<sub>k</sub>\_2La, ZnAl\_W<sub>k</sub>\_3La, ZnAl\_W<sub>k</sub>\_4La, ZnAl\_W<sub>k</sub>\_5La.

Series II was prepared via impregnation with aqueous solutions of La(NO<sub>3</sub>)<sub>3</sub> of ex-ZnAl LDH materials.

Preparation of the ZnAl LDH precursor with the composition expressed as a molar ratio of Zn/Al (0.65–0.7) was carried out by co-precipitation of ZnAl LDHs through simultaneous dosing of two streams, the (Zn(NO<sub>3</sub>)<sub>2</sub>, Al(NO<sub>3</sub>)<sub>3</sub>) aqueous solution and the Na<sub>2</sub>CO<sub>3</sub> + NaOH aqueous solution, to the precipitation reactor. Synthesis was carried out at the temperature of 75–80 °C and pH in the range of 7.5–8. The obtained residues were thoroughly washed and filtrated and then were dried at 105 °C and calcined at 500 °C for 4 h. In the subsequent stage, the materials were subjected to impregnation with aqueous solutions of lanthanum nitrate with concentrations so that the nominal La content in the final materials ranging from 1 to 9 wt% could be achieved. After rehydration, the samples were dried and calcined at 500 °C for 4 h. After drying, the prepared samples were denoted with the following symbols: ZnAl\_I\_1La, ZnAl\_I\_2La, ZnAl\_I\_3La, ZnAl\_I\_4La, ZnAl\_I\_5La, and the corresponding calcination products were denoted with the following symbols: ZnAl\_I<sub>k</sub>\_1La, ZnAl\_I<sub>k</sub>\_2La, ZnAl\_I<sub>k</sub>\_3La, ZnAl\_I<sub>k</sub>\_4La, ZnAl\_I<sub>k</sub>\_5La.

## 2.2. Material Characterization

The chemical composition of the samples was determined using the WD XRF method with an Axios mAx spectrometer (Malvern Panalytical, Malvern, UK) equipped with a 4 kW Rh SST-mAx lamp (Malvern Panalytical, Malvern, UK).

The XRD measurements were performed on an Empyrean (Malvern Panalytical, Malvern, UK) system (Bragg–Brentano geometry) equipped with a PIXcel3D detector ((Malvern Panalytical, Malvern, UK), using Cu K $\alpha$  radiation ( $\lambda = 1.542 \text{ \AA}$ ) and operating at 40 kV and 40 mA.

Fourier-transform infrared spectroscopy (FT-IR) measurements were carried out using Nicolet 8700A (Thermo Scientific, Waltham, MA, USA) equipped with a diamond crystal (Smart Orbit TR diamond ATR, Thermo Fisher Scientific, Waltham, MA, USA). Infrared spectra were obtained in the 4000–400  $\text{cm}^{-1}$  spectral range.

The thermal decomposition with evolved gas analysis (TG/DTG/EGA) studies were carried out using a STA 449 Jupiter thermal analyzer (Netzsch, Frankfurt, Germany) coupled with a QMS 430C Aëolos mass spectrometer (Netzsch, Germany). The measurements were performed in a helium stream, increasing the temperature range up to 800 °C with a rate of 10 °C/min. The changes of the sample weight and  $m/z$  signals ( $m/z = 18, 28, 30, 46$ ) were constantly monitored.

The specific surface area ( $S_{\text{BET}}$ ) and the total pore volume (TPV) were determined using an ASAP<sup>®</sup> 2050 Xtended Pressure sorption analyzer (Micromeritics Instrument Co., Norcross, GA, USA) from N<sub>2</sub> adsorption and desorption isotherms at the temperature of  $-196 \text{ °C}$  for  $p/p_0 \leq 0.99$  using the BET adsorption model and BJH (Barret–Joyner–Halenda) transformation for mesopore characteristics.

The elemental mapping (STEM–EDS) of materials was conducted using a Tecnai G2 20 X-TWIN transmission electron microscope (FEI, Hillsboro, OR, USA). The sample mapping (determination of element distribution in the sample) was carried out using STEM and recording EDS spectra from each spot corresponding to pixels of the map, point after point. The collected maps were presented as a pixel matrix with a color of the mapped element and intensity corresponding to the content of the particular element.

HRTEM images were collected using a 60–300 kV Titan G2 transmission electron microscope (FEI, Hillsboro, OR, USA) equipped with a FEG (field emission gun), a monochromator, the system of three optical condensers, objective lenses, an image corrector (Cs corrector), a HAADF detector and an EDS (energy-dispersive X-ray spectroscopy) EDAX spectrometer with a Si(Li) detector. Microscopy studies were carried out at accelerating voltage equaling to 300 kV. Phase separation (crystal lattice of ZnAl<sub>2</sub>O<sub>4</sub> and crystal lattice of ZnO) were performed with the FFT using masking available with the Gatan Digital Micrograph software package (Gatan, Inc., Pleasanton, CA, USA).

Activity in the high-temperature water–gas shift reaction (HT-WGS) was measured in the kinetic regime using a differential 4-channel reactor (conversion  $\alpha < 0.1$ ) under the following conditions: catalyst grain size (mm): 0.16–0.25, sample mass: 0.4 g, pressure (MPa): 2.5, temperature (°C): 330–400, gas flow (Ndm<sup>3</sup>/h): 60, gas composition (vol.%): CO/CO<sub>2</sub>/H<sub>2</sub> = 3.9/9.6/86.5, saturated with (H<sub>2</sub>O/gas)<sub>mol</sub> = 1.1 (steam). The stabilization time for each measurement was 2 h; then, the analyses of effluent gases were carried out using a GC (Shimadzu, Canby, OR, USA) equipped with a FID and a carbon sieve mesh: 100/120, length: 2 m, ID: 2 mm. The Shimadzu GC was calibrated for reactants (except for the steam; it was separated/condensed) from the effluent stream and a dry gas sample was injected to the GC system using certified gas mixtures containing 4/20/10 vol.% of CO/CH<sub>4</sub>/CO<sub>2</sub> from Air Liquide (Pulawy, Poland). The HT-WGS reaction rate constant was calculated using the equation:  $r_{\text{HT-WGS}} = k_0 \cdot e^{-(\Delta E/RT)} \times p_{\text{CO}}^a \times p_{\text{H}_2\text{O}}^b \times p_{\text{H}_2}^c \times p_{\text{CO}_2}^d \times (1 - \beta)$ , where:

$r_{\text{HT-WGS}}$ —WGS reaction rate (Ndm<sup>3</sup>·g<sub>cat</sub><sup>-1</sup>·h<sup>-1</sup>);

$k_0$ —preexponential factor;

$\Delta E$ —apparent activation energy;

$p_i$ —partial pressure of component “i” (MPa);

a, b, c, d—reaction order of CO, H<sub>2</sub>O, H<sub>2</sub>, CO<sub>2</sub>, respectively;

k—WGS rate constant (Ndm<sup>3</sup>·gcat<sup>-1</sup>·h<sup>-1</sup>·at<sup>-x</sup>);

β—approach to equilibrium, β is defined as pCO<sub>2</sub> × pH<sub>2</sub> × pH<sub>2</sub>O<sup>-1</sup> × pCO<sup>-1</sup> × K<sub>p</sub><sup>-1</sup>;

K<sub>p</sub>—the equilibrium constant for the WGS reaction.

The exponents for H<sub>2</sub>O, CO<sub>2</sub> and H<sub>2</sub> were in the range of 0.02 ± 0.06, -0.10 ± 0.02, -0.22 ± 0.04, respectively [22].

### 3. Results and Discussion

#### 3.1. Physicochemical Parameters of ZnAl<sub>W</sub><sub>x</sub>La and ZnAl<sub>I</sub><sub>x</sub>La Materials

Table 1 shows the total weight loss in the temperature range up to 800 °C and the temperature corresponding to the maximum rate of decomposition (T<sub>max</sub>) of ZnAl<sub>W</sub><sub>x</sub>La and ZnAl<sub>I</sub><sub>x</sub>La materials. DTG/MS patterns for the series of ZnAl<sub>W</sub><sub>x</sub>La materials are presented in Figure 1. Two major stages of decomposition processes may be distinguished from DTG/EGA curves regardless of La concentration: low- (100–200 °C) and medium-temperature processes (210–410 °C). H<sub>2</sub>O and CO<sub>2</sub> are the only decomposition products. Regardless of the lanthanum content, all the materials undergo complete thermal decomposition in the temperature range up to 410 °C. In the first stage, physically bound water is desorbed and simultaneous dehydration of interlayer spaces takes place, which is evidenced with an intensive m/z = 18 signal coming from water and a lack of distinct EGA m/z = 44 bands corresponding to CO<sub>2</sub>. In the second stage, in the range up to 410 °C, dehydroxylation of brucite-like layers and decarbonization with the release of CO<sub>2</sub> take place. Less intense and sharp DTG bands are observed for the increased La content.

**Table 1.** The weight loss up to 800 °C (TG) and the temperature of the highest decomposition rate (T<sub>max</sub>) for ZnAl<sub>W</sub><sub>x</sub>La and ZnAl<sub>I</sub><sub>x</sub>La materials.

Sample	TG (%)	T <sub>max</sub> Decomposition Rate (°C)	Sample	TG (%)	T <sub>max</sub> Decomposition Rate (°C)
ZnAl <sub>W</sub> _1La	24.5	289	ZnAl <sub>I</sub> <sub>k</sub> _1La	12.7	164
ZnAl <sub>W</sub> _2La	24.7	284	ZnAl <sub>I</sub> <sub>k</sub> _2La	13.6	153
ZnAl <sub>W</sub> _3La	24.6	291	ZnAl <sub>I</sub> <sub>k</sub> _3La	13.7	199
ZnAl <sub>W</sub> _4La	25.4	284	ZnAl <sub>I</sub> <sub>k</sub> _4La	14.9	206
ZnAl <sub>W</sub> _5La	25.5	284	ZnAl <sub>I</sub> <sub>k</sub> _5La	16.9	240

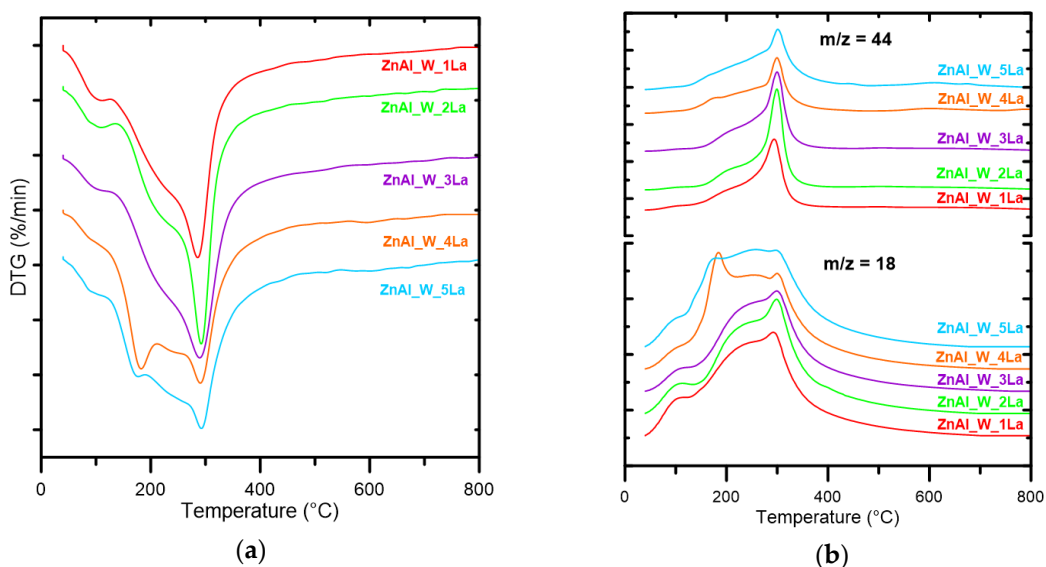


**Figure 1.** DTG (a) and EGA (b) curves for the series of ZnAl<sub>W</sub><sub>x</sub>La materials.

DTG/MS patterns of ZnAl\_I\_xLa series are presented in Figure 2a,b. Thermal decomposition of ZnAl\_I\_xLa series is more complex and proceeds at higher temperatures (100–680 °C). Three major stages can be distinguished: low- (100–200 °C), middle- (200–450 °C) and high-temperature (450–680 °C). Gaseous products of decomposition are H<sub>2</sub>O, CO<sub>2</sub> and nitrogen oxide with the corresponding signals  $m/z = 30$  (NO) and  $m/z = 46$  (NO<sub>2</sub>). In the first stage, the release of H<sub>2</sub>O and simultaneous dehydration of interlayer spaces proceeds. In the next stage (200–450 °C), dehydration and decomposition of carbonates and nitrates intercalated between the layers of rehydrated ex-hydrotalcite-like mixed Zn–Al–La oxides take place.

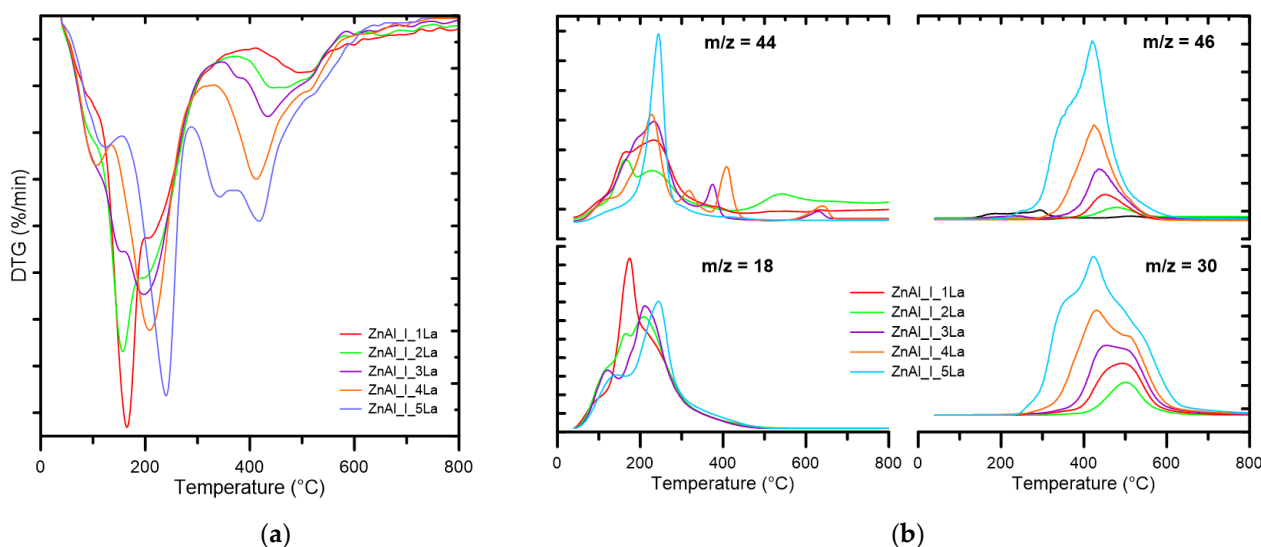


**Figure 2.** DTG (a) and EGA (b) curves for the series of ZnAl\_I\_xLa materials.

The intensity increase of bands  $m/z = 30$  and  $m/z = 46$  is observed with the increase in lanthanum content and a significant increase and shift of maximum intensity towards lower temperatures. They correspond to nitrogen oxides being the products of thermal decomposition of lanthanum nitrate. The third stage involves further decomposition of  $\text{NO}_3^-$  anions with the release of NO and NO<sub>2</sub>. The processes occurring over 600 °C have low intensity and are accompanied by CO<sub>2</sub> release from decomposition of durable carbonates, the so called high-temperature carbonates (HT-CO<sub>3</sub>). In case of the ZnAl\_I\_xLa series, we observed the memory effect involving the recovery of the primary layer structure of the precursor as a result of the contact between the Zn–Al mixed oxide and the aqueous solution of lanthanum salt.

The amount of La added has an impact on the reconstruction process of meixnerite-like and hydrotalcite-like layer structures. Moreover, with the increase in La content, durability of these structures also increases, which is reflected in a slight but noticeable increase of decomposition temperatures for these materials (see Table 1).

### 3.2. Structural and Textural Properties of ZnAl\_W\_xLa and ZnAl\_I\_xLa Materials

The XRD patterns of ZnAl\_W\_xLa series are presented in Figure 3a. For the series of ZnAl\_W\_xLa materials, a well-structured phase of the hydrotalcite-like structure of the formula  $\text{Zn}_{0.6}\text{Al}_{0.4}(\text{OH})_{0.2} \cdot 0.5\text{H}_2\text{O}$  is dominant, which is evidenced by characteristic peaks at  $2\theta$  11.7°, 23.6°, 34.7°, 60.5°, corresponding to the diffraction on the planes (003), (012), (110), (113), respectively. Additionally, for materials with the highest content of La (ZnAl\_W\_4La, ZnAl\_W\_5La), planes (015), (018) and (113) are exposed at  $2\theta$  39.1°, 46.6°, 61.6°. All the materials also contain complex zinc carbonate ( $\text{Zn}_5(\text{CO}_3)_2 \cdot (\text{OH})_6$ ) as evidenced by the characteristic peaks at  $2\theta$  12.8°, 19.2° and 26.5° and trace amounts of ZnO. No phases corresponding to lanthanum compounds for the whole range of lanthanum

content of the ZnAl<sub>k</sub>W<sub>x</sub>La series were found. It can be concluded that La was incorporated in the ZnAl LDH lattice.

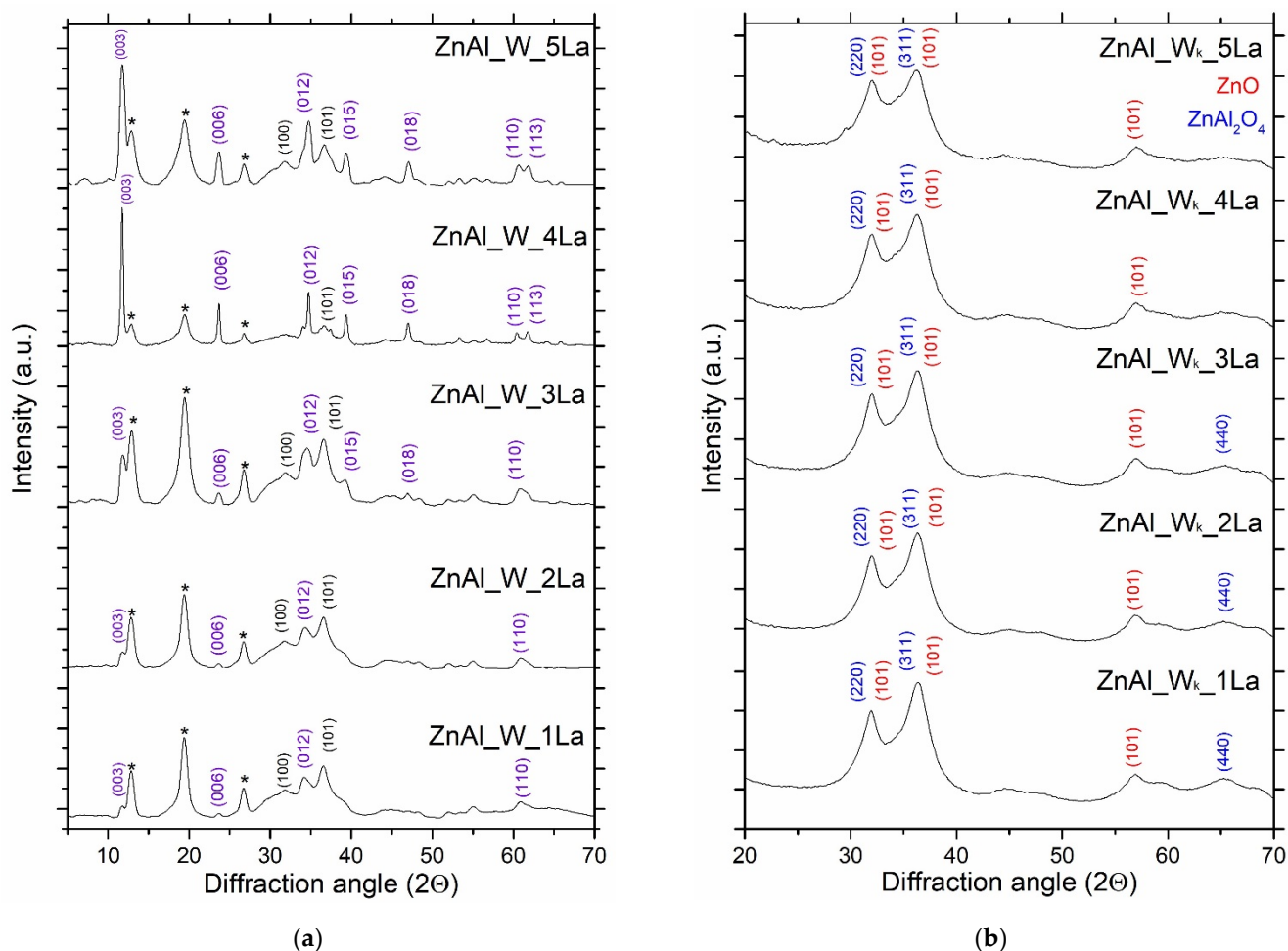


**Figure 3.** XRD patterns of ZnAl<sub>W<sub>x</sub></sub>La (a) and ZnAl<sub>W<sub>k</sub></sub>La (b) materials: Zn<sub>0.6</sub>Al<sub>0.4</sub>(OH)<sub>0.2</sub>·0.5H<sub>2</sub>O phase peaks at 2θ 11.7° (003), 23.6° (006), 34.7° (012), 39.1° (015), 46.6° (018), 60.5° (110) and 61.6° (113); 11.79°, 23.69°, 34.78°, 39.47° (015), 46.6° (018), 60.5° (110), 61.6° (113); (\*) Zn<sub>5</sub>(CO<sub>3</sub>)<sub>2</sub>(OH)<sub>6</sub> phase peaks at 2θ 12.8°, 19.2° and 26.5°; ZnO phase peaks at angles 2θ 31.8° (100), 36.1° (101).

The peaks characteristic of ZnAl LDH materials disappeared after calcination at 500 °C due to the collapse of lamellar structures (Figure 3b). In the phase composition of ZnAlLa<sub>W<sub>k</sub></sub>La materials, diffraction peaks at 2θ 31.2°, 36.7°, 65.0° and at 34.4°, 36.3° were observed, which are characteristic of nanocomposites of poorly crystallized mixed oxides (both ZnO and ZnAl<sub>2</sub>O<sub>4</sub>). No phases corresponding to lanthanum compounds in materials of the ZnAl<sub>W<sub>k</sub></sub>La series were found. Additionally, with the increase in the La content, peak broadening was observed, which indicates the decrease in the degree of nanocrystallinity of the mixed oxides.

As presented in Table S1, there was no influence of the lanthanum content on the size of ZnAl<sub>2</sub>O<sub>4</sub> nanocrystallites. However, with the increase in the La content, a clear effect of decrease in the ZnO crystallite size was observed. The crystallinity decrease was probably caused by partial amorphization of ZnO. These observations are consistent with the data presented in the literature [15]. No phases corresponding to lanthanum oxides for the whole range of the lanthanum content of the ZnAl<sub>W<sub>k</sub></sub>La series were found. It can be concluded that La was incorporated in the bulk zinc aluminate spinel framework.

For ex-hydrotalcite-like mixed Zn–Al oxides (ZnAl<sub>I</sub>-xLa), due to impregnation with the aqueous lanthanum nitrate solution and drying at 105 °C (Figure 4a), the reconstruction of the layered structure was visible, which was demonstrated with the presence of peaks characteristic of the hydrotalcite analog at 2 $\theta$  11.7° (003), 23.6° (006), 34.3° (012), 39.3° (015), 47° (018). Moreover, for the material of the highest La content (ZnAl<sub>I</sub>-5La), peaks at 2 $\theta$  9.9°, 19.9°, 34.3°, 37.7°, 43.4°, 61.1° were identified, which confirmed the presence of complex basic nitrates of Zn and Al. It showed that the applied conditions of thermal processing (500 °C) of ZnAl LDHs do not lead to irreversible changes of the formed heterostructural ZnO/ZnAl<sub>2</sub>O<sub>4</sub> mixed oxides. ZnO/ZnAl<sub>2</sub>O<sub>4</sub> nanocomposites recalcined at 500 °C exhibit the capacity to recover the primary layered structure of LDHs by rehydration with aqueous La(NO<sub>3</sub>)<sub>3</sub> nitrate.

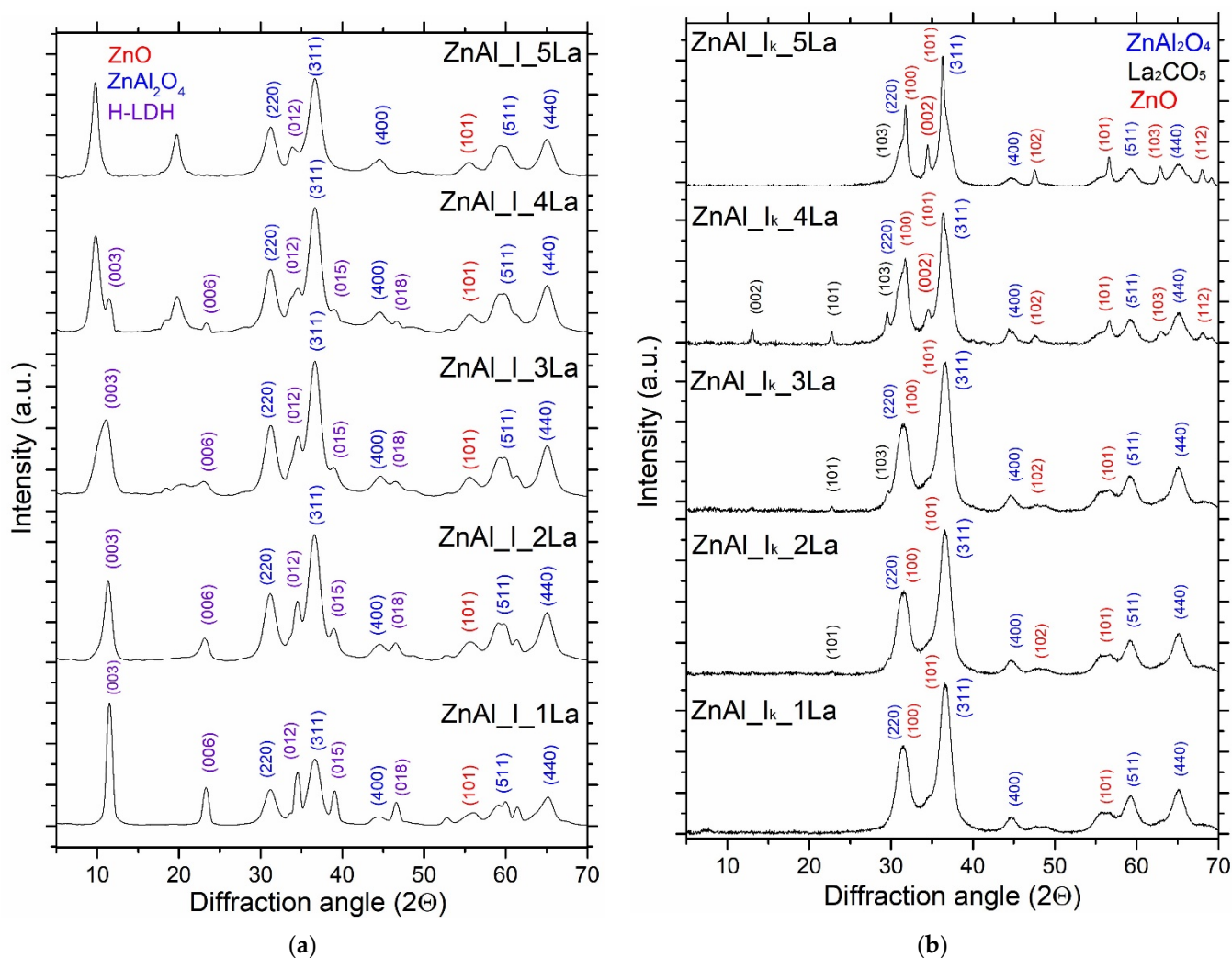


Figure 4. XRD pattern of the ZnAl<sub>I</sub>-xLa (a) and ZnAl<sub>I<sub>k</sub></sub>-xLa (b) materials.

Quite different XRD patterns correspond to the ZnAl<sub>I<sub>k</sub></sub>-xLa materials (Figure 4b). No phases originating from lanthanum compounds were identified for the materials of both the ZnAl<sub>I<sub>k</sub></sub>-1La and ZnAl<sub>I<sub>k</sub></sub>-2La series indicating that the La content in the studied materials is too low or that lanthanum has been partially incorporated into the Zn–Al spinel structure simultaneously with the rehydration process. However, for a higher La content (ZnAl<sub>I<sub>k</sub></sub>-3La, ZnAl<sub>I<sub>k</sub></sub>-4La), lanthanum is crystallized as La<sub>2</sub>CO<sub>5</sub>, which is demonstrated with the appearance of weak reflections for angles 2 $\theta$  13.1°, 22.9° and 29.5°. Relatively narrow peaks at 2 $\theta$  31.2°, 36.7°, 44.6°, 59.1°, 65.0° corresponding with diffraction planes of (220), (311), (400), (511), (440) were observed, which can be attributed to ZnAl<sub>2</sub>O<sub>4</sub>. It

is worth noticing that for a higher content of La, the appearance of additional peaks at  $2\theta$   $36.3^\circ$ ,  $68.0^\circ$  corresponding to diffraction on planes (002), (103), (112) characteristic of the ZnO phase is visible.

As presented in Table S1, an evident effect of lanthanum content on ZnO nanocrystalite size (from 2.5 to 11.9 nm) was observed. The consequence of increase in the ZnO nanocrystalite size is a visible asymmetry of these peaks at  $31.17^\circ$ – $33^\circ$  and  $35^\circ$ – $39^\circ$ , indicating the presence of  $\text{La}_2\text{O}_3$ –ZnO/ $\text{ZnAl}_2\text{O}_4$  mixed oxides. With the increase of the La content, there is an increased asymmetry between these peaks. However, splitting of heterojunction structures of mixed oxides  $\text{La}_2\text{O}_3$ –ZnO/ $\text{ZnAl}_2\text{O}_4$  was not observed.

However, with the increase of the La content, no change in the size of  $\text{ZnAl}_2\text{O}_4$  nanocrystalites was observed.

The structural properties of the  $\text{ZnAl}_k\text{W}_k\text{xLa}$  and  $\text{ZnAl}_k\text{I}_k\text{xLa}$  materials were also investigated by FT-IR (see Figure 5a,b). For the series of  $\text{ZnAl}_k\text{W}_k\text{xLa}$  and  $\text{ZnAl}_k\text{I}_k\text{xLa}$  materials, bands at a wavenumber range of  $3700$ – $2800\text{ cm}^{-1}$  were attributed to O–H bonds characteristic of surface OH groups.

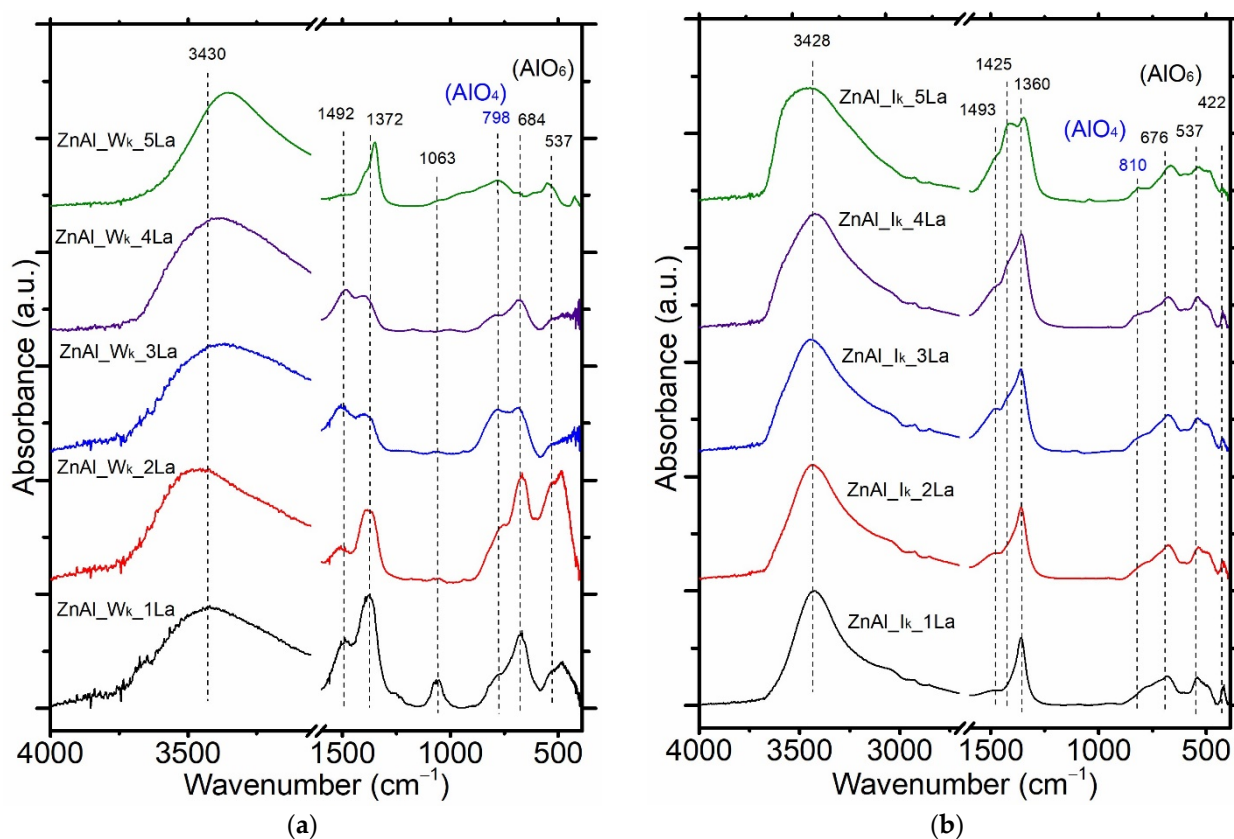


Figure 5. FT-IR spectra of the  $\text{ZnAl}_k\text{W}_k\text{xLa}$  (a) and  $\text{ZnAl}_k\text{I}_k\text{xLa}$  (b) series of materials.

For the series of  $\text{ZnAl}_k\text{W}_k\text{xLa}$  materials, the bands at  $1372$  and  $1492\text{ cm}^{-1}$  characteristic of  $\text{CO}_3^{2-}$  stretching vibrations were evidenced. In case of the  $\text{ZnAl}_k\text{I}_k\text{xLa}$  samples, the bands at wavenumbers of  $1550$ – $1300\text{ cm}^{-1}$  characteristic of antisymmetric stretching vibrations of  $\text{CO}_3^{2-}$  intercalated between the layers of the ex-hydraltalcite-like mixed Zn–Al oxides were visible. The intensity of these bands changed with the increase of the La content. As presented in Figure 5a for the series of  $\text{ZnAl}_k\text{W}_k\text{xLa}$  materials, asymmetry of bands located in the range of  $550$ – $850\text{ cm}^{-1}$  indicates the presence of Al coordinated as  $\text{AlO}_6$  or  $\text{AlO}_4$ . Bands at  $684\text{ cm}^{-1}$  and  $537\text{ cm}^{-1}$  corresponded to stretching vibrations of Al–O, whereas the band at  $422\text{ cm}^{-1}$  could be attributed to bending O–Al–O bonds with octahedral coordination ( $\text{AlO}_6$ ). Bands at  $798\text{ cm}^{-1}$  corresponded to Al–O bonds with tetrahedral coordination ( $\text{AlO}_4$ ). However, with the increase of the La content, the

decrease of bands mentioned was evidenced, which suggests the structural evolution of ZnO–ZnAl<sub>2</sub>O<sub>4</sub>. For the series of ZnAl-I<sub>k</sub>-xLa samples, the intensity of the bands located in the range of 550–850 cm<sup>-1</sup> was relatively low.

Table 2 shows the total La content (wt%) for the series of ZnAl-W<sub>k</sub>-xLa and ZnAl-I<sub>k</sub>-xLa materials and the content of Zn and Al expressed with the Zn/Al molar ratio. The desired concentrations of the modifier and main components were verified by means of XRF measurements. For the series of ZnAl-W<sub>k</sub>-xLa and ZnAl-I<sub>k</sub>-xLa materials, a good agreement between the actual and nominal composition was achieved. Additionally, Table 2 presents textural parameters of ZnAl-W<sub>k</sub>-xLa and ZnAl-I<sub>k</sub>-xLa. The modification of the ZnAl-W<sub>k</sub>-xLa series by introduction of a small amount of La via coprecipitation led to insignificant changes of textural properties. Both changes of the specific surface area and pore volume due to lanthanum compound addition (from 0.9 to 8.5 wt% La) were of inconclusive nature. The series of ZnAl-W<sub>k</sub>-xLa materials with a relatively large specific surface area (in the range from 150 to 162 m<sup>2</sup>/g) and pore volume (in the range from 0.29 to 0.34 cm<sup>3</sup>/g) were obtained. For the series of ZnAl-I<sub>k</sub>-xLa materials (La incorporated by impregnation), significantly smaller specific surface areas were obtained, including more than twice as small (for 8.7 wt% La–ZnAl-I<sub>k</sub>-5La) in comparison with the materials prepared via the coprecipitation route. As the La content increased, the specific surface area decreased significantly, while the total pore volume increased. At relatively low concentrations of lanthanum (1.9–2.8 wt%), beneficial influence of La on the total pore volume increase was revealed. However, with further increase of the lanthanum content, the opposite effect was observed, i.e., the TPV decrease.

**Table 2.** Chemical composition and textural properties of the ZnAl-W<sub>k</sub>-xLa and ZnAl-I<sub>k</sub>-xLa series of materials.

Sample	wt% La <sup>a</sup>	(Zn/Al) <sub>mol</sub> <sup>a</sup>	S <sub>BET</sub> (m <sup>2</sup> /g)	TPV <sup>b</sup> (cm <sup>3</sup> /g)	MPV <sub>BJH</sub> <sup>c</sup> (cm <sup>3</sup> /g)
ZnAl-W <sub>k</sub> -1La	0.9	0.68	158	0.34	0.34
ZnAl-W <sub>k</sub> -2La	1.7	0.67	162	0.3	0.3
ZnAl-W <sub>k</sub> -3La	2.4	0.7	160	0.29	0.29
ZnAl-W <sub>k</sub> -4La	4.3	0.66	162	0.3	0.3
ZnAl-W <sub>k</sub> -5La	8.5	0.66	154	0.32	0.32
ZnAl-I <sub>k</sub> -1La	0.9	0.7	100	0.25	0.25
ZnAl-I <sub>k</sub> -2La	1.9	0.68	98	0.27	0.27
ZnAl-I <sub>k</sub> -3La	2.8	0.67	90	0.35	0.35
ZnAl-I <sub>k</sub> -4La	4.6	0.69	89	0.27	0.27
ZnAl-I <sub>k</sub> -5La	8.7	0.68	76	0.22	0.22

<sup>a</sup> Determined by XRF; <sup>b</sup> total pore volume determined by the Barret–Joyner–Halenda method; <sup>c</sup> mesopore volume determined by the Barret–Joyner–Halenda method.

Tzompantzi et al. [16] studied the effect of Zn–Al modification by introduction of La at the stage of ZnAlLa LDH precursor synthesis via precipitation with the urea route and thermal treatment. Oxide materials obtained by calcination of the Zn–Al–La LDH precursor at 400 °C exhibited a significantly smaller surface area but an increased pore volume with an increase in the La<sub>2</sub>O<sub>3</sub> content. Liu et al. [14] observed that for low content of La, the specific surface area appeared to be significantly smaller as compared to the reference ZnAl<sub>2</sub>O<sub>4</sub>, but further La content increase (at least 10 wt%) caused the reverse effect, that is, a significant specific surface area increase. The beneficial effect of La on the volume and average pore size was also observed. Authors relate this fact to the positive effect of La on the activity of modified ZnAl<sub>2</sub>O<sub>4</sub> spinels in the trans-esterification reaction.

The pore size distributions for the series of ZnAl-W<sub>k</sub>-xLa and ZnAl-I<sub>k</sub>-xLa materials are presented in Figure S1. The pore systems of both the ZnAl-W<sub>k</sub>-xLa and ZnAl-I<sub>k</sub>-xLa series were complex and comprised three types of pores: mesopores with the diameter ranging from 2 to 10 nm, wide mesopores with a dominant diameter of 40–45 nm and macropores with a dominant diameter of 130–140 nm. The materials of ZnAl-W<sub>k</sub>-xLa were

characterized by a lower total pore volume as compared to the materials of ZnAl<sub>k</sub>-xLa series and a similar pore distribution.

### 3.3. Surface Morphology of Mixed Oxides Obtained from ZnAlLa LDHs and ex-ZnAl LDHs

STEM-EDS images of selected materials of the ZnAl<sub>k</sub>-xLa and ZnAl<sub>k</sub>-I<sub>k</sub>-xLa series are presented in Figures S2–S5. The STEM-EDS elemental maps show dispersion of Zn (yellow), Al (violet), O (red) in the investigated series of materials. Moreover, La (light blue) coverage and surface location are presented. STEM-EDS results for ZnAl<sub>k</sub>-1La (Figure S2) indicate good dispersion of Zn and Al and a relatively uniform distribution of lanthanum over the surface of heterostructural mixed oxide nanoparticles. In case of higher concentrations of lanthanum (Figure S3), EDS maps revealed an apparently larger lanthanum surface coverage of nanoparticles of mixed oxides related to the intensity of the turquoise color on the EDS maps. Moreover, small agglomerates are locally visible.

XRD and DTG results showed that mixed oxides are capable of reconstructing the original LDH layer structure upon contact with an aqueous solution and a variety of anions can be intercalated into the recovered LDHs. Since the rehydration process, semi-homogenous distribution of La was evidenced in final materials. STEM-EDS studies of ZnAl<sub>k</sub>-1La and ZnAl<sub>k</sub>-5La materials showed significant differences in distribution. In case of ZnAl<sub>k</sub>-1La, lanthanum nanoparticles were well dispersed. Relatively uniform distribution of lanthanum was present in the form of fine aggregates over the surface of mixed oxide nanoparticles. Lanthanum was distributed over ZnO nanoparticles and also decorated zinc aluminate spinel nanoparticles. For ZnAl<sub>k</sub>-5La, the EDS maps showed non-uniform distribution and local agglomeration of lanthanum species.

The surface microstructure and morphology of the ZnAl<sub>k</sub>-xLa and ZnAl<sub>k</sub>-I<sub>k</sub>-1La materials were investigated by HR-TEM (Figure S6 and S7). The series of ZnAl<sub>k</sub>-xLa materials exhibited the needle morphology (see Figure S2). Some particles joined together to form elongated agglomerates.

More detailed analysis of the ZnAl<sub>k</sub>-1La materials by phase identification and separation revealed the particles of ZnO and ZnAl<sub>2</sub>O<sub>4</sub> with a very small diameter (1–5 nm). Clear widening of the rings (Figure 6a) as well as broadening of XRD diffraction peaks (Figures 3a and 6a) show low crystallinity of the material. With the increase of the lanthanum content, the surface morphology of the ZnAl<sub>k</sub>-xLa series was changed. For ZnAl<sub>k</sub>-3La (Figure 7a,b), heterojunction structures of ZnO/ZnAl<sub>2</sub>O<sub>4</sub> which are composed of ZnAl<sub>2</sub>O<sub>4</sub> nanoparticles with an interplanar distance of 2.86 Å (220), 2.44 Å (311) and ZnO nanoparticles with an interplanar distance of 2.48 Å, 2.81 Å and lattice planes (100), (101) were visible. For ZnAl<sub>k</sub>-5La, there were zinc-enriched areas in which very small ZnO nanoparticles were clearly segregated on the surface of zinc aluminate spinel nanoparticles. As presented in Figure 8a,b, the increase in the La content leads to the formation of amorphous ZnO on the ZnAl<sub>2</sub>O<sub>4</sub> surface (see Figure 3b).

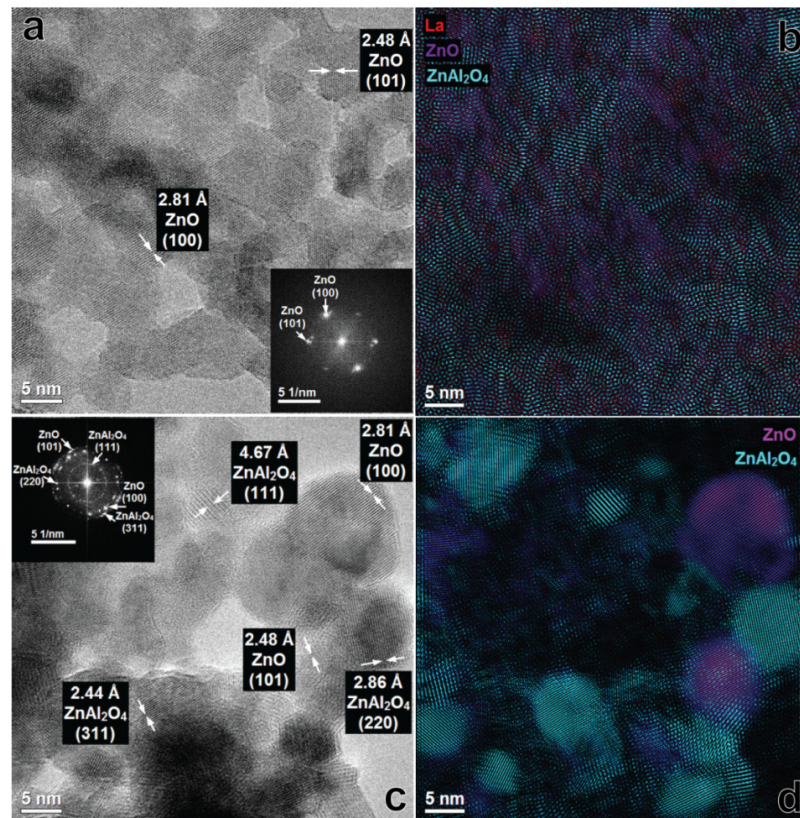


**Figure 6.** HRTEM image and FFT with phase identification of ZnAl<sub>Wk</sub>\_1La (a,b) and ZnAl<sub>Ik</sub>\_1La (c,d).

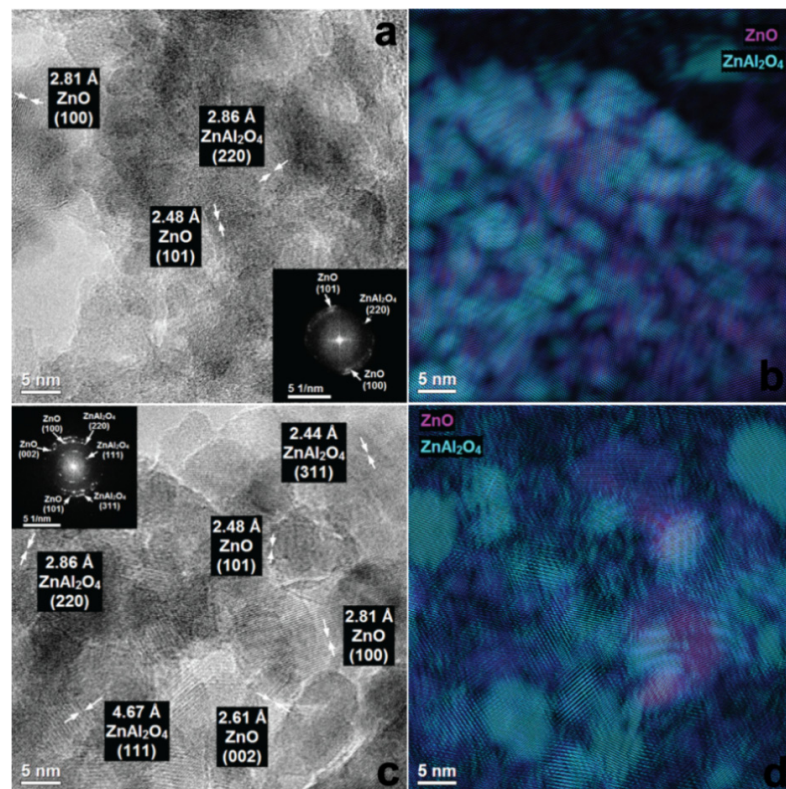


**Figure 7.** HRTEM images and FFT with phase identification of ZnAl<sub>Wk</sub>\_3La (a,b) and ZnAl<sub>Ik</sub>\_3La (c,d).

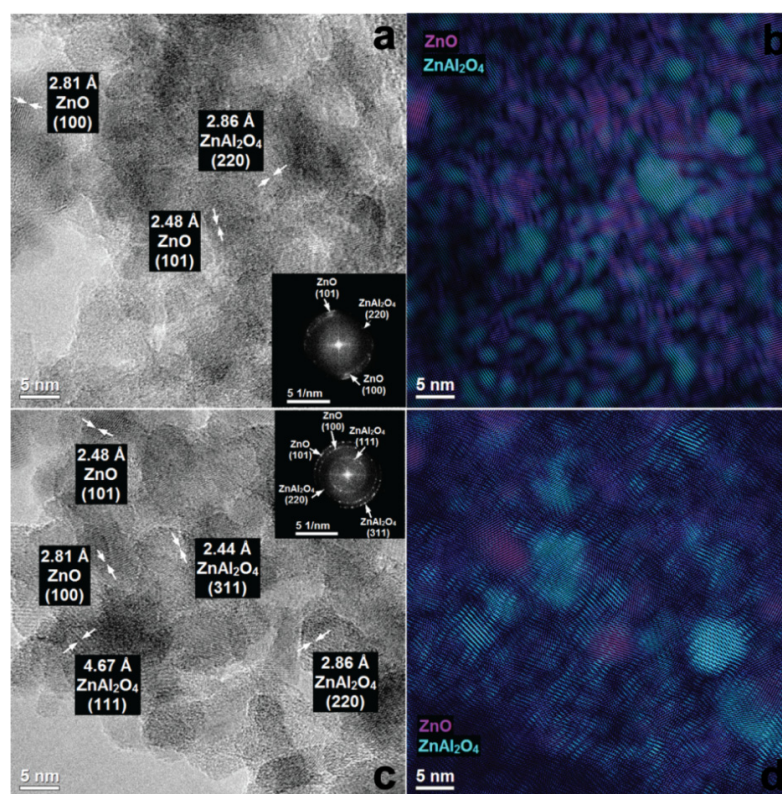


**Figure 8.** HRTEM images and FFT with phase identification of ZnAl<sub>Wk</sub>\_5La (a,b) and ZnAl<sub>Ik</sub>\_5La (c,d).

Phase identification and separation data analysis showed that no crystalline phases containing lanthanum were detected. It suggests that lanthanum is built into the zinc aluminate spinel framework.

The morphology of ZnAl<sub>Ik</sub>\_1La materials was substantially different from the ZnAl<sub>Wk</sub>\_xLa materials (see Figure S7 and Figure 6c,d). The ZnAl<sub>Ik</sub>\_1La material was composed of heterostructural nanocomposites with a more or less regular, round shape. One can distinguish nanoparticles of relatively large ZnO ((101) 2.48 Å, (100) 2.81 Å) and ZnAl<sub>2</sub>O<sub>4</sub> ((111) 4.67 Å, (220) 2.86 Å, (311) 2.44 Å). With the increase of the lanthanum content (Figure 7c,d), the surface morphology of the ZnAl<sub>Ik</sub>\_xLa samples was changed. There were relatively large nanoparticles of ZnAl<sub>2</sub>O<sub>4</sub> and ZnO, as well as zinc aluminate spinel nanoparticles which were partially covered with ZnO particles. As presented in Figure 8c,d for ZnAl<sub>Ik</sub>\_5La, distinct phase segregation of ZnO on ZnAl<sub>2</sub>O<sub>4</sub> was observed. We speculate that the increase in the La content leads to the formation of segregated ZnO on the surface of ZnAl<sub>2</sub>O<sub>4</sub>.

### 3.4. Evaluation of ZnO/Zn(AlLa)<sub>2</sub>O<sub>4</sub> and La-ZnO/ZnAl<sub>2</sub>O<sub>4</sub> Mixed Oxides in the High-Temperature Water–Gas Shift Reaction

The catalytic activity of ZnO/Zn(AlLa)<sub>2</sub>O<sub>4</sub> and La-ZnO/ZnAl<sub>2</sub>O<sub>4</sub> mixed oxides in the HT-WGS was studied within the temperature range of 350–420 °C. Table 3 presents HT-WGS reaction rate constants for the ZnAl<sub>Wk</sub>\_xLa and ZnAl<sub>Ik</sub>\_xLa materials. The series of ZnAl<sub>Wk</sub>\_xLa and ZnAl<sub>Ik</sub>\_xLa mixed oxides presented a similar activity level in the HT-WGS reaction at 350 °C (at 350 °C, the reaction rate constant of series II is, on average, greater by ca. 30%). The differences of rate constant values for particular ZnAl<sub>Wk</sub>\_xLa and ZnAl<sub>Ik</sub>\_xLa materials were more visible at higher temperatures (370–420 °C).

**Table 3.** The comparison of HT-WGS rate constants for the series of ZnAl<sub>W<sub>k</sub></sub>xLa and ZnAl<sub>I<sub>k</sub></sub>xLa materials.

Samples	Average HT-WGS Rate Constants $k$ ( $\text{Ndm}^3 \cdot \text{g}_{\text{cat}}^{-1} \cdot \text{h}^{-1} \cdot \text{at}^{-0.95}$ )			
	350 °C	370 °C	400 °C	420 °C
ZnAl <sub>W<sub>k</sub></sub> _1La	1.5	4.8	7.9	11.3
ZnAl <sub>W<sub>k</sub></sub> _2La	1.9	3.1	8	11.9
ZnAl <sub>W<sub>k</sub></sub> _3La	1.9	4.6	9.9	12
ZnAl <sub>W<sub>k</sub></sub> _4La	2.2	4.8	10.5	12.6
ZnAl <sub>W<sub>k</sub></sub> _5La	2.5	5	10.3	13.3
ZnAl <sub>I<sub>k</sub></sub> _1La	2.8	5.2	9.9	12.5
ZnAl <sub>I<sub>k</sub></sub> _2La	2.9	5.7	11.5	14.1
ZnAl <sub>I<sub>k</sub></sub> _3La	2.3	4.9	11	13.8
ZnAl <sub>I<sub>k</sub></sub> _4La	2.4	4.4	7.8	8.3
ZnAl <sub>I<sub>k</sub></sub> _5La	2.3	3.5	5.6	7

For the content of La increased up to 1.9–2.8 wt%, the catalytic activity for the series of ZnAl<sub>I<sub>k</sub></sub>xLa materials significantly increased. For ZnAl<sub>I<sub>k</sub></sub>\_2La and ZnAl<sub>I<sub>k</sub></sub>\_3La, reaction rate constants at 420 °C have the value of approx. 14.1 and 13.8 ( $\text{Ndm}^3 \cdot \text{g}_{\text{cat}}^{-1} \cdot \text{h}^{-1} \cdot \text{at}^{-0.95}$ ), respectively. The increase of the lanthanum content (above 2.8 wt%) leads to adverse effects, i.e., to the decrease of reaction rate constants.

The catalytic activity for the series of ZnAl<sub>W<sub>k</sub></sub>xLa and ZnAl<sub>I<sub>k</sub></sub>xLa materials is related to the La content and is primarily related to the method of doping with lanthanum. The activity of materials containing 2.8 wt% La prepared by deposition of a La compound on the surface of mixed oxides via impregnation is higher by approx. 30% as compared to materials with the same content of a dopant but obtained using the coprecipitation method. The reverse effect was found for materials with a higher content of La, i.e., 4.6 and 8.7 wt% La. For such La content, the catalytic activity of materials obtained via the coprecipitation technique was higher by approx. 40% and 50% as compared to impregnated ones. Based on the achieved results, it can be concluded that ZnO segregation on the ZnAl<sub>2</sub>O<sub>4</sub> surface leads to a lower catalytic activity in the HT-WGS comparing to the heterojunction structure of ZnO/Zn(AlLa)<sub>2</sub>O<sub>4</sub>.

#### 4. Conclusions

The way of lanthanum addition and incorporation route into the Zn–Al system plays a fundamental role in the location of lanthanum (bulk or/and surface) in final mixed oxides (ZnO/Zn(AlLa)<sub>2</sub>O<sub>4</sub> or La<sub>2</sub>O<sub>3</sub>–ZnO/ZnAl<sub>2</sub>O<sub>4</sub>) and in creating the structure and surface morphology of the systems which determine the catalytic activity. Addition of La via coprecipitation allowed for a better distribution of La in the bulk and surface of the zinc aluminate spinel comparing to La incorporation via the impregnation technique. The right amount of La is crucial because with the lanthanum content above 2.8 wt%, distinct phase segregation of ZnAl<sub>2</sub>O<sub>4</sub> to ZnO is observed on the surface of mixed oxides.

Deep changes in the structure of ex-ZnAl LDH materials due to calcination at 500 °C lead to the formation of heterostructural nanocomposites (ZnO/Zn(AlLa)<sub>2</sub>O<sub>4</sub>) with a structural memory. This feature reveals partial reconstruction of the original structure of a hydroxalite analog due to impregnation by aqueous solutions of lanthanum nitrates with different concentrations.

The activity toward the HT-WGS reaction of ZnO/Zn(Al,La)<sub>2</sub>O<sub>4</sub> and La<sub>2</sub>O<sub>3</sub>–ZnO/ZnAl<sub>2</sub>O<sub>4</sub> mixed oxides is related to the La content. The surface ZnO segregation causes a decrease of catalytic activity in the HT-WGS. Such systems exhibit lower activity than materials containing the heterojunction structure of ZnO/Zn(AlLa)<sub>2</sub>O<sub>4</sub> as the dominant component. However, they are base materials for designing complex multicomponent systems for a series of chemical reactions, i.e., eco-friendly catalysts for the water–gas shift reaction.

**Supplementary Materials:** The following are available online at <https://www.mdpi.com/article/10.3390/ma14082082/s1>, Figure S1: Pore size distribution of the ZnAl<sub>1</sub>W<sub>k</sub>-xLa and ZnAl<sub>1</sub>I<sub>k</sub>-xLa materials; Figure S2: TEM images of the ZnAl<sub>1</sub>W<sub>k</sub>-xLa and ZnAl<sub>1</sub>I<sub>k</sub>-xLa materials; Figure S3: TEM images of the ZnAl<sub>1</sub>W<sub>k</sub>-xLa and ZnAl<sub>1</sub>I<sub>k</sub>-xLa materials; Figure S4: STEM-EDS images along with detailed maps of La (turquoise), Zn (yellow), Al (purple), and O (red) distributions of the ZnAl<sub>1</sub>I<sub>k</sub>-1La material; Figure S5: STEM-EDS images along with detailed maps of La (turquoise), Zn (yellow), Al (purple), and O (red) distributions of the ZnAl<sub>1</sub>I<sub>k</sub>-5La material; Figure S6: TEM images of ZnAl<sub>1</sub>W<sub>k</sub>-xLa materials; Figure S7: TEM images of ZnAl<sub>1</sub>I<sub>k</sub>-xLa materials; Table S1: Effect of La addition and incorporation route on the size of ZnO and ZnAl<sub>2</sub>O<sub>4</sub> crystallites.

**Author Contributions:** Conceptualization: K.A.-J.; Methodology: K.A.-J., P.K. and G.S.; software: K.A.-J., W.P., R.B. and G.S.; supervision, K.A.-J.; writing—original draft preparation: K.A.-J.; review and editing, P.K., W.P., R.B. and G.S.; investigation: K.A.-J., W.P., R.B. and G.S. All authors have read and agreed to the published version of the manuscript.

**Funding:** The research was supported by the National Science Centre, Poland, within the SONATA program under grant No. 2017/26/D/ST5/01211.

**Institutional Review Board Statement:** Not applicable.

**Informed Consent Statement:** Not applicable.

**Data Availability Statement:** Data is contained within the article.

**Acknowledgments:** The authors thank W. Sofińska-Chmiel for her FT-IR analysis. The research was carried out with the equipment purchased with the financial support of the European Regional Development Fund in the framework of the Polish Innovation Economy Operational Program (contract No. POIG.02.01.00-06024/09, Center of Functional Nanomaterials).

**Conflicts of Interest:** The authors declare no conflict of interest.

## References

1. Ertl, G.; Knözinger, H.; Weitkam, J. *Preparation of Solid Catalysts*; John Wiley & Sons: Weinheim, NY, USA, 2012.
2. Xu, M.; Wie, M. Layered Double Hydroxide-Based Catalysts: Recent Advances in Preparation, Structure, and Applications. *Adv. Funct. Mater.* **2018**, *28*, 1802943. [[CrossRef](#)]
3. Zhang, G.; Zhang, X.; Meng, Y.; Pan, G.; Ni, Z.; Xia, S. Layered Double Hydroxides-based Photocatalysts and Visible-light-driven Photodegradation of Organic Pollutants: A Review. *Chem. Eng. J.* **2020**, *392*, 123684. [[CrossRef](#)]
4. Zhang, Y.; Zhang, L.; Hu, L.; Huang, S.; Jin, Z.; Zhang, M.; Huang, X.; Lu, J.; Ruana, S.; Zeng, Y.J. Multifunctional Zn–Al layered double hydroxides for surface-enhanced Raman scattering and surface-enhanced infrared absorption. *Dalton Trans.* **2019**, *48*, 426–434. [[CrossRef](#)] [[PubMed](#)]
5. Auerbach, S.M.; Carrado, K.A.; Dutta, P.K. *Handbook of Layered Materials*; Marcel Dekker: New York, NY, USA, 2004.
6. Elhalil, A.; Elmoubarki, R.; Farnane, M.; Machrouhi, A.; Mahjoubi, F.Z.; Sadiq, M.; Qourzal, S.; Abdennouri, M.; Barka, N. Novel Ag-ZnO-La<sub>2</sub>O<sub>2</sub>CO<sub>3</sub> photocatalysts derived from the Layered Double Hydroxide structure with excellent photocatalytic performance for the degradation of pharmaceutical compounds. *J. Sci. Adv. Mater. Devices* **2019**, *4*, 34–46. [[CrossRef](#)]
7. Carriazo, D.; Domingo, C.; Martin, C.; Rives, V. Structural and Texture Evolution with Temperature of Layered Double Hydroxides Intercalated with Paramolybdate Anions. *Inorg. Chem.* **2006**, *45*, 1243. [[CrossRef](#)] [[PubMed](#)]
8. Mei-Yu, G.; Dong-Mei, X.; Yu-Fei, S.; Guo, Y. ZnO/ZnAl<sub>2</sub>O<sub>4</sub> prepared by calcination of ZnAl layered double hydroxides for ethanol sensing. *Sens. Actuators B* **2013**, *188*, 1148.
9. Sun, Y.; Zhou, Y.; Wang, Z.; Ye, X. Structural and morphological transformations of Zn–Al layered double hydroxides through hydrothermal treatment. *Appl. Surf. Sci.* **2009**, *255*, 6372–6377. [[CrossRef](#)]
10. Giannakas, A.E.; Ladavos, A.K.; Armatas, G.S.; Petrakis, D.E.; Pomonis, P.J. Effect of composition on the conductivity of CTAB–butanol–octane–nitrate salts (Al(NO<sub>3</sub>)<sub>3</sub> + Zn(NO<sub>3</sub>)<sub>2</sub>) microemulsions and on the surface and textural properties of resulting spinels ZnAl<sub>2</sub>O<sub>4</sub>. *Appl. Surf. Sci.* **2006**, *252*, 2159–2170. [[CrossRef](#)]
11. Zhao, Y.; Chen, G.; Bian, T.; Zhou, C.; Waterhouse, G.I.N.; Wu, L.Z.; Tung, C.H.; Smith, L.J.; O’Hare, D.; Zhang, T. Defect-Rich Ultrathin ZnAl-Layered Double Hydroxide Nanosheets for Efficient Photoreduction of CO<sub>2</sub> to CO with Water. *Adv. Mater.* **2015**, *27*, 7824–7831. [[CrossRef](#)] [[PubMed](#)]
12. Valle, B.; Aramburu, B.; Remiro, A.; Bilbao, J.; Gayubo, A.G. Effect of calcination/reduction conditions of Ni/La<sub>2</sub>O<sub>3</sub>–Al<sub>2</sub>O<sub>3</sub> catalyst on its activity and stability for hydrogen production by steam reforming of raw bio-oil/ethanol. *Appl. Catal. B Environ.* **2014**, *147*, 402–410. [[CrossRef](#)]
13. Bicki, R.; Antoniuk-Jurak, K.; Michalska, K.; Franczyk, E.; Konkol, M.; Kowalik, P.; Pańczyk, M.; Ryczkowski, J.; Słowik, G.; Borowiecki, T. The effect of La<sub>2</sub>O<sub>3</sub> and CeO<sub>2</sub> modifiers on properties of Ni–Al catalysts for LNG prereforming. *Int. J. Hydrogen Energy* **2021**, *46*, 11664–11676. [[CrossRef](#)]

14. Liu, Q.; Wang, L.; Wang, C.; Qu, W.; Tian, Z.; Ma, H.; Wang, D.; Wang, B.; Xu, Z. The effect of lanthanum doping on activity of Zn-Al spinel for transesterification. *Appl. Catal. B Environ.* **2013**, *136–137*, 210–217. [[CrossRef](#)]
15. Xie, X.; An, X.; Wang, X.; Wang, Z. Preparation, Characterization and Application of ZnAlLa-Hydrotralcite-like Compounds. *J. Nat. Gas Chem.* **2003**, *12*, 259–263.
16. Tzompantzi, F.; Mendoza-Damian, G.; Rici, J.L.; Mantilla, A. Enhanced photoactivity for phenol mineralization on ZnAlLa mixed oxides prepared from calcined LDHs. *Catal. Today* **2014**, *220–222*, 56–60. [[CrossRef](#)]
17. Tzompantzi, F.; Carrera, Y.; Morales-Mendoza, G.; Valverde-Aguilar, G.; Mantilla, A. ZnO–Al<sub>2</sub>O<sub>3</sub>–La<sub>2</sub>O<sub>3</sub> layered double hydroxides as catalysts precursors for the esterification of oleic acid fatty grass at low temperature. *Catal. Today* **2013**, *212*, 164–168. [[CrossRef](#)]
18. Shariatinia, Z.; Bagherpour Sardasahra, F. Synthesis and characterization of novel spinel Zn<sub>1.114</sub>La<sub>1.264</sub>Al<sub>0.5</sub>O<sub>4.271</sub> nanoparticles. *J. Alloys Compd.* **2016**, *686*, 384–393. [[CrossRef](#)]
19. Khani, F.Y.; Bahadoran, S.; Soltanali, J.; Ahari, S. Hydrogen production by methanol steam reforming on a cordierite monolith reactor coated with Cu–Ni/LaZnAlO<sub>4</sub> and Cu–Ni/γ-Al<sub>2</sub>O<sub>3</sub> catalysts. *Res. Chem. Intermed.* **2018**, *44*, 925–942. [[CrossRef](#)]
20. Khani, F.Y.; Bahadoran, N.; Safari, S.; Soltanali, S.; Taheri, A. Hydrogen production from steam reforming of methanol over Cu-based catalysts: The behavior of Zn<sub>x</sub>La<sub>x</sub>Al<sub>1-x</sub>O<sub>4</sub> and ZnO/La<sub>2</sub>O<sub>3</sub>/Al<sub>2</sub>O<sub>3</sub> lined on cordierite monolith reactors. *Int. J. Hydrogen Energy* **2019**, *44*, 11824–11837. [[CrossRef](#)]
21. Antoniak-Jurak, K.; Kowalik, P.; Michalska, K.; Próchniak, W.; Bicki, R. Zn-Al Mixed Oxides Decorated with Potassium as Catalysts for HT-WGS: Preparation and Properties. *Catalysts* **2020**, *10*, 1094. [[CrossRef](#)]
22. Antoniak-Jurak, K.; Kowalik, P.; Michalska, K.; Franczyk, E.; Mrozek, A. WGS reaction empirical kinetics over novel potassium promoted ZnAlLa mixed oxides catalyst. *Chem. Eng. Res. Des.* **2020**, *164*, 293–298. [[CrossRef](#)]